# Instability and Large Scale Circulations in a Two-Column Model of the Tropical Troposphere

David J. Raymond and Xiping Zeng

Physics Department and Geophysical Research Center

New Mexico Tech

Socorro, NM 87801 USA

raymond@kestrel.nmt.edu

Submitted to *Quart. J. Roy. Meteor. Soc.*

December 10, 2005

# Summary

A two-column model of the tropical atmosphere is developed. The two columns are kept in buoyancy equilibrium by mass exchange driven by the inter-column pressure gradient, and diabatic processes are parameterized by highly simplified schemes. This model is used to investigate whether spontaneous large-scale circulations will develop in the tropical atmosphere when the sea surface temperature and solar radiative forcing are uniform. Such circulations do indeed develop in the model, with ascent in one column and descent in the other, when one of the columns is slightly perturbed from the initial state of radiative-convective equilibrium. A key element of the circulation dynamics is that increased equivalent potential temperature in a column leads to enhanced convection and rainfall in that column, which further increases the equivalent potential temperature there. The latter effect arises because convection enhances surface heat fluxes and decreases outgoing longwave radiation by virtue of the increase in stratiform cloudiness. These results form an attractive explanation for the observed patchiness of deep convection over warm tropical oceans and suggest that further modeling and observational work be directed toward understanding the budget of equivalent potential temperature in the tropical atmosphere and its relationship to rainfall.

# 1 Introduction

Given spatially uniform sea surface temperature (SST) and solar forcing, will large-scale circulations involving deep convection develop in the tropical troposphere? This is a fundamental question which remains unanswered in tropical meteorology.

Observations would seem to favor an affirmative answer to the above question. SST is a rough guide to the existence of deep convection over tropical oceans, in the sense that deep convection only occurs when the SST exceeds some threshold which is of order 26° C - 27° C. However, once the SST exceeds this threshold, it loses its predictive value. Waliser and Graham (1993) showed that the highest SSTs tend to be associated with much less deep convection than slightly more modest values. As Gray (1973) indicated, only of order 20% of the warm-water regions of the tropics are covered by heavily precipitating deep convection, the rest experiencing either convection of low precipitation efficiency or no deep convection at all. Thus, something besides SST must be organizing the distribution of deep convection over warm tropical oceans. The organizing mechanism may be an instability of some kind which results in the partitioning of these regions into areas of enhanced and suppressed convection. However, an alternate possibility is that middle latitude variability is overflowing into the tropics and influencing the distribution of deep convection there. A better understanding of the factors controlling tropical deep convection is thus needed to answer the above question.

Theory and modeling so far have been of little help with respect to this question, partly because different treatments of diabatic processes lead to such different results, e. g., Raymond (1994), Chao and Lin, (1994), Yano, McWilliams, and Moncrieff (1996), and partly because most numerical simulations to date have included factors such as latitudinally varying Coriolis parameter or imposed large scale forcing of some kind (Xu and Arakawa, 1992; Xu, Arakawa, and Krueger, 1992). These factors impose their own organizing principles and thus confound attempts to recognize self-organization by convection.

Note that we consider convective forcing to be thermodynamic rather than dynamic

in nature, i. e., we aren't concerned with how conditionally unstable parcels are lifted to the level of free convection. On sufficiently small space and time scales, dynamic forcing is important, and self-sustaining convective systems are known to be possible as long as thermodynamic conditions remain favorable (see, e. g., Rotunno and Klemp, 1985; Rotunno, Klemp, and Weisman, 1988). However, ultimately thermodynamics must dominate on sufficiently large scales (Raymond, 1995).

The analysis of dry convection is facilitated by the fact that the variable which governs the buoyancy of parcels, namely the potential temperature, is also conserved in internal convective processes. The amount of convection is thus a function of the strength of non-conservative processes which destabilize the environmental profile of potential temperature.

For moist convection, potential temperature, which still governs buoyancy (except for virtual temperature effects), is not conserved. The equivalent potential temperature is (nearly) conserved by moist convection, but it is not directly related to the buoyancy. Thus, a theoretical model of moist convection is necessarily more difficult than for dry convection.

Common sense would suggest that there ought to be at least a rough relationship between the humidity of the atmosphere and the propensity for precipitation to occur. There are a number of reasons for this. Entrained dry air promotes the dissipation of cumulus clouds, and it also can lead to the evaporation of rain before it reaches the surface. Ferrier, Simpson, and Tao (1996) showed that environmental humidity is an important factor in the precipitation efficiency of numerically modeled deep convection.

Convection by itself cannot change the equivalent potential temperature of parcels, but it can redistribute parcels in the atmosphere. In particular, deep convective downdrafts tend to transport low equivalent potential air downward from mid-levels, thus reducing its value at low levels, as shown by Zipser (1969). This reduces the humidity of air at low levels.

Postulating these two effects, namely the strong dependence of precipitation rate on

humidity and the tendency of deep convection to reduce humidity, one can imagine a feedback process in which the tendency of precipitating convection to dry the atmosphere is just balanced by the tendency of other processes to moisten it. If the time scale for these tendencies to adjust the humidity is short compared to the time scale of interest, the humidity profile will tend to remain near the equilibrium profile in which these opposing tendencies are in balance. This is a variation on the convective quasi-equilibrium hypothesis of Arakawa and Schubert (1974). Building on the work of Neelin and Held (1987), Raymond (2000b) showed under certain more or less plausible assumptions that the adjustment time for humidity is of order a day or less in a region of pre-existing heavy precipitation, whereas it can be much longer in regions which are clear and dry.

The balance discussed above has a further consequence. If a net source of equivalent potential temperature develops in a region, then the convection and precipitation rate must increase in order to maintain the above balance. Thus, the net source of equivalent potential temperature controls the amount of convection and precipitation.

Neelin and Held (1987) defined a parameter called the gross moist stability (GMS) as the ratio of the moist static energy transport through a region of convection to the mass transport through the region. The GMS is thus the mean increase in the moist static energy of parcels passing through the convection. We adopt here an alternative definition of GMS as the mean increase in equivalent potential temperature of a parcel passing through convection. The GMS is a measure of the efficiency with which the net source of equivalent potential temperature produces moist ascent and precipitation. Smaller values mean that a given equivalent potential temperature source produces more of these quantities.

In the absence of radiation, surface fluxes, and dissipative processes, the GMS will be zero, as there would be no processes which could alter a parcel's equivalent potential temperature. Figure 1 shows the dominant processes which change the equivalent potential temperature in deep convective areas relative to clear regions. Surface latent and sensible heat fluxes are often enhanced in convective regions due to downdraft air coming

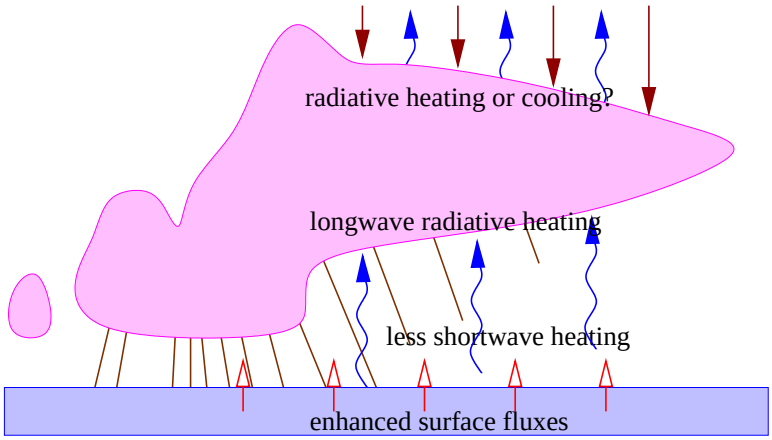


Figure 1: Two processes increase equivalent potential temperature in deep convective areas relative to clear regions, namely, enhanced surface sensible and latent heat fluxes and the absorption of longwave radiation by stratiform cloud bases. On the other hand, interception of shortwave radiation by clouds reduces heating in the lower troposphere. The net effect of longwave cooling and solar heating at cloud top is uncertain at this point due to uncertainties in shortwave radiative absorption there.

in contact with the surface, and due to the enhanced gustiness of winds in such regions (Zipser, 1969). Furthermore, the bases of convectively produced stratiform clouds intercept upwelling longwave radiation. This can result in strong, localized radiative heating at these cloud bases, relative to clear regions (Albrecht and Cox, 1975).

The interception of downwelling shortwave radiation by high clouds reduces radiative heating by shortwave absorption in the lower half of the troposphere. According to Cox and Griffith (1979), this reduction at low levels in convectively active regions is equal to about half of the increase in heating due to the increased absorption of upwelling longwave radiation. It is partially compensated by cloud absorption of shortwave radiation at high levels.

The source of equivalent potential temperature divides naturally into two parts, an externally forced part and a part which is associated with the presence of convective clouds. External contributors to enhanced surface heat fluxes are high SSTs and externally generated strong boundary layer winds. Layer clouds advected in from elsewhere can also affect the radiation balance so as to generate an equivalent potential temperature source. Internally generated contributors are enhanced surface fluxes due to the action of convective downdrafts and the above-described effects of locally produced stratiform cloudiness.

High SSTs and strong surface winds are well-known contributors to deep convection and precipitation over warm oceans in agreement with the above predictions. Less well understood is the degree to which convectively produced anomalies in the equivalent potential temperature source are themselves effective in generating additional deep precipitating convection. If internal production is effective in this way, then we have a potential feedback mechanism which can lead to the development of a large-scale instability and the spontaneous partitioning of the atmosphere over warm tropical oceans into regions of active and suppressed convection. Raymond (2000a) found that the equivalent potential temperature source produced by cloud-radiation interactions was sufficient to generate an intertropical convergence zone in a zonally symmetric model even when the

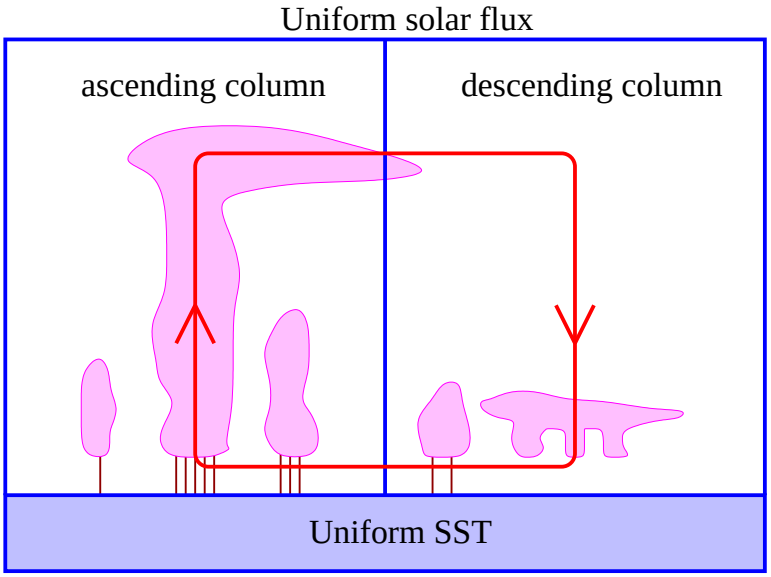


Figure 2: Representation of a tropical circulation in a homogeneous environment by a two column idealization.

SST is meridionally uniform.

This paper explores the efficacy of the above feedback process in the context of a two-column model of tropical circulations similar to that proposed by Pierrehumbert (1995) and Nilsson and Emanuel (1999). In particular, we pose the following question: Imagine two atmospheric columns, each of which represents the mean conditions in a homogenous region with a horizontal scale much larger than a single convective system. If the columns have identical SSTs, solar inputs, etc., and are initially in radiative-convective equilibrium, will a perturbation to one of the columns intensify or decay with time? If the two-column system is unstable in that the perturbation grows with time, then it is likely that the tropical atmosphere will exhibit a similar instability.

The fundamental idea of a two column model is that gravity waves rapidly redistribute buoyancy anomalies in the deep tropics, so that density differences between neighboring regions of ascent and descent are minimal, at least above the atmospheric boundary layer. The regions exchange mass as a result of gravity wave action so as to

relax toward zero density or pressure difference between them at each level. The result is a vertical circulation between the two regions, as illustrated in figure 2.

As Mapes (1993) showed, the differing speeds of gravity waves with different vertical wavelengths makes the actual adjustment toward buoyancy equilibrium at any given level a complex function of the vertical normal mode structure of the excited gravity waves. The replacement of this process by a simple relaxation is therefore an idealization which approximates the actual process only in the long-time limit. A consequence is that the simulated density differences between the two columns are not necessarily representative of those occurring in the real world, and only those inter-column differences which are independent of those density differences are physically significant. This is a significant caveat regarding models of this type.

The diabatic processes in our two-column model are represented using the diabatic parameterizations of Raymond and Torres (1998) as modified and extended by Raymond (2000a). Section 2 describes the model and a small extension made to the radiation parameterization to take into account the existence of fractional cloud coverage in each column. In section 3 we demonstrate that the model is unstable in the sense described above, whether cloud-radiation interactions are taken into account or not, though the instability is stronger when such interactions are turned on. In section 4 the mechanisms of this instability are analyzed in terms of the equivalent potential temperature budget. Conclusions and a discussion are presented in section 5.

# 2 Model

In this section the two column model is developed. The anelastic governing equations in geometrical coordinates for mean density $\rho(z)$, equivalent potential temperature $\theta_e$, and total water mixing ratio $r_t$ (vapor plus advected condensate) are

$$\frac{\partial}{\partial z}(\rho w) = -\nabla \cdot (\rho \mathbf{u}) \tag{1}$$

$$\frac{\partial \rho \theta_e}{\partial t} + \frac{\partial}{\partial z}(\rho \theta_e w) = -\nabla \cdot (\rho \theta_e \mathbf{u}) + \rho S_e \tag{2}$$

$$\frac{\partial \rho r_t}{\partial t} + \frac{\partial}{\partial z}(\rho r_t w) = -\nabla \cdot (\rho r_t \mathbf{u}) + \rho S_r \tag{3}$$

where $\mathbf{u}$ is the horizontal wind, $w$ is the vertical wind, $\nabla$ is the horizontal gradient, and $S_e$ and $S_r$ are the convective tendencies of equivalent potential temperature and total water mixing ratio.

In all two column models, terms like $\nabla \cdot (\rho \mathbf{u})$ must somehow be approximated. If the two column model is representing the flows in two regions of a non-rotating environment, then the net effect of the explicit dynamics of the model must be to drive the two columns toward buoyancy equilibrium with each other. To the extent that this buoyancy equilibrium is reached, the exact choice of mechanism should not be important. Therefore, we choose a mechanism derived from scaling the horizontal momentum equation in a non-rotating environment:

$$\frac{\partial \rho u}{\partial t} = -\frac{\partial p}{\partial x} + \ldots, \tag{4}$$

where $u$ is the horizontal wind and $p$ is the pressure, and where nonlinear terms have been neglected. Assuming a horizontal scale of $\Delta x$ and approximating the time derivative by Newtonian relaxation on a time scale $\tau$, the above equation becomes

$$\rho U \approx -\frac{\tau(p_r - p)}{\Delta x}, \tag{5}$$

where $p$ and $p_r$ are respectively the pressures in the test and reference columns and $U$ is the wind blowing from the test to the reference column. The pressure in each column is obtained from integrating the hydrostatic equation down from a common pressure value at the top of the domain.

In the present work the equivalent potential temperature is defined

$$\theta_e = \theta \exp(er) \tag{6}$$

where $\theta$ is the potential temperature, $r$ is the water vapor mixing ratio, and $e = (L_c + L_f)/(C_p T_R)$. The quantities $L_c$ and $L_f$ are the latent heats of condensation and freezing, $C_p$ is the specific heat of air at constant pressure, and $T_R = 300$ K is a constant reference

temperature. We also make the approximation $r \approx r_t$, which means that the grid scale liquid water is ignored. The convective parameterization rapidly removes liquid water, so this approximation is quite accurate. The potential temperature profile in each column can be computed from $\theta_e$ and $r_t$ using the above approximation, from which the pressure profile can also be computed using the hydrostatic law.

Making the further approximation $\nabla \cdot (\rho \mathbf{u}) \approx \rho U/\Delta x$, we have

$$E \equiv -\nabla \cdot (\rho \mathbf{u}) \approx \mu(p_r - p), \tag{7}$$

where

$$\mu \equiv \tau/(\Delta x)^2 \tag{8}$$

is the inter-column coupling constant.

Similar treatments for the corresponding terms in the equivalent potential temperature and total water equations yield

$$-\nabla \cdot (\rho \theta_e \mathbf{u}) \approx < \theta_e > E, \tag{9}$$

$$-\nabla \cdot (\rho r_t \mathbf{u}) \approx < r_t > E, \tag{10}$$

where $< \theta_e >$ and $< r_t >$ are the values of $\theta_e$ and $r_t$ on the edge of the test column. If there is no horizontal mean wind, then the flow is either all inward ($\mathbf{u} \cdot \mathbf{n} < 0$) or all outward ($\mathbf{u} \cdot \mathbf{n} > 0$) at each level. In the former case one can replace $< \theta_e >$ and $< r_t >$ by their reference column values, which we call $\theta_{er}$ and $r_{tr}$. On the other hand, for outward flow the values of $\theta_e$ and $r_t$ on the area boundary are equal to their test column values, or just $\theta_e$ and $r_t$.

If there is horizontal advection, then ventilation of the column will occur, with the flow partly into the test column and partly out at each level. In this case estimating $< \theta_e >$ and $< r_t >$ is more complex. It is difficult to account for ventilation in a two column model, so we ignore this possibility here.

Using the above ideas, the governing equations (2) and (3) can be recast as equations for the test column:

$$\frac{\partial \rho \theta_e}{\partial t} + \frac{\partial}{\partial z}(\rho \theta_e w) = < \theta_e > E + \rho S_e, \tag{11}$$

and

$$\frac{\partial \rho r_t}{\partial t} + \frac{\partial}{\partial z}(\rho r_t w) =< r_t > E + \rho S_r. \tag{12}$$

One additional piece of information is needed to close the system, namely the vertical velocity in the test column. This may be obtained from the anelastic mass continuity equation:

$$w = \frac{1}{\rho}\int_0^z E dz'. \tag{13}$$

So far we have assumed that the reference column is infinite in extent, which means that the values of variables in the reference column remain fixed. However, we can extend the analysis to the case of a reference column of finite area by adding evolution equations for this column. If the ratio of the areas of the test and reference columns is $\epsilon$, then these equations take the form

$$\frac{\partial \rho \theta_{er}}{\partial t} + \frac{\partial}{\partial z}(\rho \theta_{er} w_r) = -\epsilon < \theta_e > E + \rho S_{er} \tag{14}$$

and

$$\frac{\partial \rho r_{tr}}{\partial t} + \frac{\partial}{\partial z}(\rho r_{tr} w_r) = -\epsilon < r_t > E + \rho S_{rr} \tag{15}$$

where by mass continuity we have

$$\rho w_r = -\epsilon \rho w. \tag{16}$$

The potential temperature and mixing ratio source terms in the reference column are denoted $S_{er}$ and $S_{rr}$.

The usual interpretation of $\tau$ in the context of Newtonian relaxation is that of a dissipative time constant. However, as discussed in the introduction, the mechanism for adjustment of neighboring atmospheric columns in the tropics is more likely to be gravity wave propagation. An alternate interpretation of $\tau$ is the time required for a gravity wave to propagate out of the test column and into the reference column. If $\Delta x$ is interpreted as the size of the test column and $c$ is the speed of gravity wave propagation, then we have

$$\tau \approx \Delta x / c, \tag{17}$$

and

$$\mu = 1/(c\Delta x). \tag{18}$$

Thus, for example, if $c = 50$ m s$^{-1}$ and $\Delta x = 2000$ km, then $\mu = 10^{-5}$ ks km$^{-2}$. This corresponds to a relaxation time of $\tau = \Delta x/c \approx 40$ ks, or about half a day. This is much shorter than the large scale dissipation times usually assumed for the tropics, which suggests that gravity wave adjustment rather than dissipation dominates, at least for length scales of a few thousand kilometers.

The radiation model of Raymond and Torres (1998) simulates the emission and absorption of thermal infrared radiative fluxes by clouds by adding a cloud absorption coefficient $\kappa_c$ to the clear air absorption coefficient $\kappa_i$ in the optical depth equation for each radiation channel $i$:

$$d\tau_i = \rho(C_i\kappa_i + r_l\kappa_c)dz, \tag{19}$$

where $r_l$ is the condensed water mixing ratio. If the condensed water consists of spherical droplets of uniform radius $R$, and if the radiative flux consists only of vertically propagating beams of radiation, then

$$\kappa_c = 3/(4R\rho_w), \tag{20}$$

where $\rho_w$ is the mass density of condensed water. If, more realistically, radiation is close to isotropic, then the value of $\kappa_c$ will be somewhat bigger for the same condensed water distribution.

About 20% of the downwelling solar radiation is absorbed by the clear atmosphere (Liou, 1980). In the Raymond-Torres model, this solar fraction is treated like thermal radiation, in that it is not scattered. (See Raymond and Torres, 1998, for details.) Clouds absorb this downwelling radiation in the model when they are present, causing a certain amount of solar heating of cloud tops to occur. The magnitude of this effect in nature is unclear at this point, due to uncertainties in our knowledge of cloud absorption processes (Cess, et al., 1995; Ramanathan, et al., 1995; Stephens, 1996; Cess and Zhang, 1996; Valero, et al., 1997; Cess, et al., 1999).

Of possibly greater dynamical importance is the absorption of upwelling longwave radiation by the undersides of opaque mid-level stratiform clouds. The resulting heating has a large effect on the equivalent potential temperature budget in the tropical troposphere. The opacity of such cloud layers greatly reduces the uncertainties in longwave radiative heating — basically, all upwelling radiation is dumped in a layer near cloud base, the exact thickness of which is unimportant as long as it is considerably less than the cloud depth.

Another problem with the Raymond-Torres radiation parameterization is that each grid box is assumed to have uniform cloud coverage. This grossly overestimates the radiative effects of clouds in many cases, since it is rare for a region the size of the grid box of a global model to be uniformly covered with high cloud. We solve this problem here by assuming instead that some fixed fractional area $f_c$ of each grid box is covered by clouds. Radiative calculations at each time step are done twice in each grid box, once with clouds and once without. The net effect on the grid box is then taken to be the average of the radiative effects in the cloudy and clear regions weighted respectively by $f_c$ and $1 - f_c$.

The model is run by integrating the finite difference analogs of equations (7) and (11) - (16) forward in time. The vertical domain is about 20 km, the vertical cell size a uniform 0.75 km, and the time step 0.5 ks. Upstream differencing in flux form (Smolarkiewicz, 1983) is used to integrate the equations. Comparisons with more sophisticated schemes show that the diffusive property of upstream differencing isn't particularly detrimental to the present calculations, since diffusion only occurs when vertical motion and hence vertical transport already exists. Furthermore, upstream differencing tends to suppress certain numerical instabilities which develop out of the interaction between the explicit integration and the diabatic parameterizations.

| Parameter | Value | Meaning |
|---|---|---|
| $T_{SS}$ | 300 K | Sea surface temperature |
| $U_{eff}$ | 5 m s$^{-1}$ | Effective surface wind speed |
| $C_D$ | 0.001 | Drag coefficient |
| $\lambda_s$ | 0.1 ks$^{-1}$ | Stratiform rain constant |
| $\lambda_p$ | $2 \times 10^{-5}$ ks$^{-1}$ | Convective rain constant |
| $\lambda_e$ | 200 ks$^{-1}$ | Evaporation constant |
| $R$ | 10 $\mu$m | Effective drop radius |

Table 1: Model parameters for the calculations in this paper. The effective surface wind speed is $U_{eff} = (U^2 + W^2)^{1/2}$, where $U$ is the actual wind speed and $W$ is the gustiness parameter, as defined by Raymond and Torres (1998).

# 3 Stability of coupled columns

We now ask whether two coupled columns initially in radiative-convective equilibrium return to this equilibrium state following a perturbation to the mixing ratio profile of one of the columns of the following form:

$$r_t(z) = r_0(z)[1 + H(z/z_s)\exp(1 - z/z_s)], \tag{21}$$

where $r_0(z)$ is the radiative-convective equilibrium profile of mixing ratio, $z_s = 3$ km, and $H$ is 0.1. We present a set of simulations with different values of the inter-column coupling parameter $\mu$, assuming that $\epsilon = 1$, so that the subsidence region is the same size as the ascent region. We employ the model parameters shown in table 1.

We test for instability with $\kappa_c = 75000$ m$^3$ kg$^{-1}$ km$^{-1}$, which reflects an effective radius for cloud particles of $R = 10$ $\mu$m. Values of the inter-column coupling constant are set to $\mu = (1, 2, 5, 10, 20, 50) \times 10^{-6}$ ks km$^{-2}$. Three different cases with different cloud fractions are investigated, namely with $f_c = (0, 0.5, 1.0)$.

Instability develops in the model with cloud radiation interactions both off ($f_c = 0$) and on ($f_c = 0.5, 1.0$). Figure 3 shows the evolution of the precipitation in the test

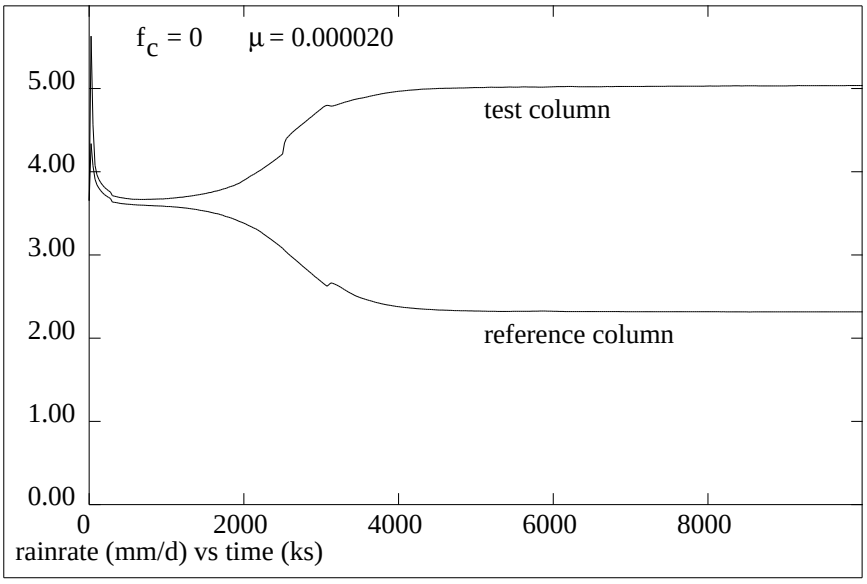


Figure 3: Evolution of rainfall rates in the test and reference columns for the case with $f_c = 0$ and $\mu = 20 \times 10^{-6}$ ks km$^{-2}$.

and reference columns for $f_c = 0$ and $\mu = 20 \times 10^{-6}$ ks km$^{-2}$. Approximately 4000 ks ($\approx$ 45 d) is required in this case for the rainfall rates in the two columns to relax to equilibrium.

Figure 4 shows the mass flux $M$ between the two columns, calculated as the vertical integral of the positive part of $E$,

$$M = \int_{E>0} E dz, \tag{22}$$

for all test cases. Larger values of $\mu$ lead to shorter relaxation times in all cases. Stronger cloud-radiation interactions (as indicated by larger values of $f_c$) lead to much shorter relaxation times as well, with relaxation occurring in periods as short as $\approx$ 700 ks (about 8 d) for the largest values of $\mu$ and $f_c$.

The difference between the test and reference column equilibrium rainfall rates is a good measure of the strength of the circulation between the two columns. Figure 5 shows this difference as a function of $\log(\mu)$ for $f_c = (0, 0.5, 1.0)$. In all cases the difference is essentially zero for small values of $\mu$. Thus, columns of sufficiently large lateral dimen-

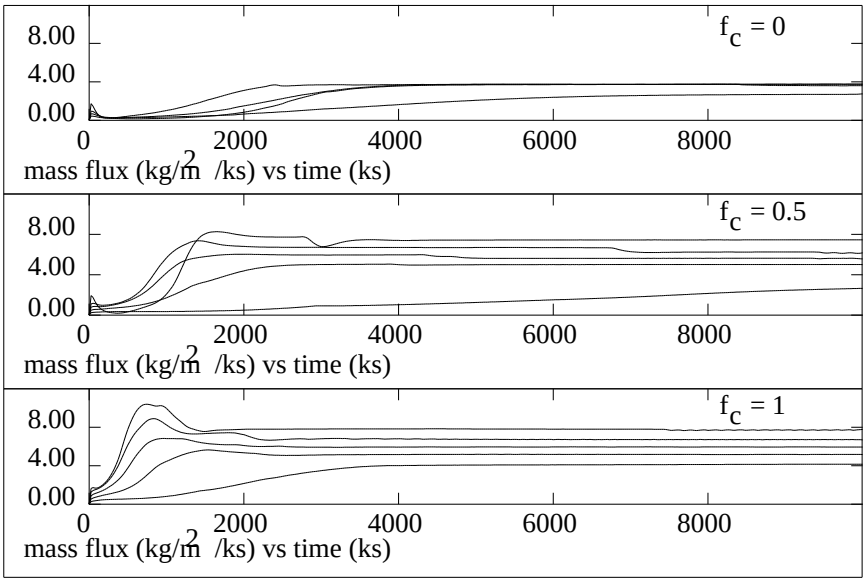


Figure 4: Evolution of mass flux $M$ in the circulation between the columns as a function of time for all cases which exhibited instability. The different values of $\mu$ corresponding to each curve are not labeled to avoid clutter, but larger values of $\mu$ lead to shorter relaxation times and larger equilibrium values in all cases.

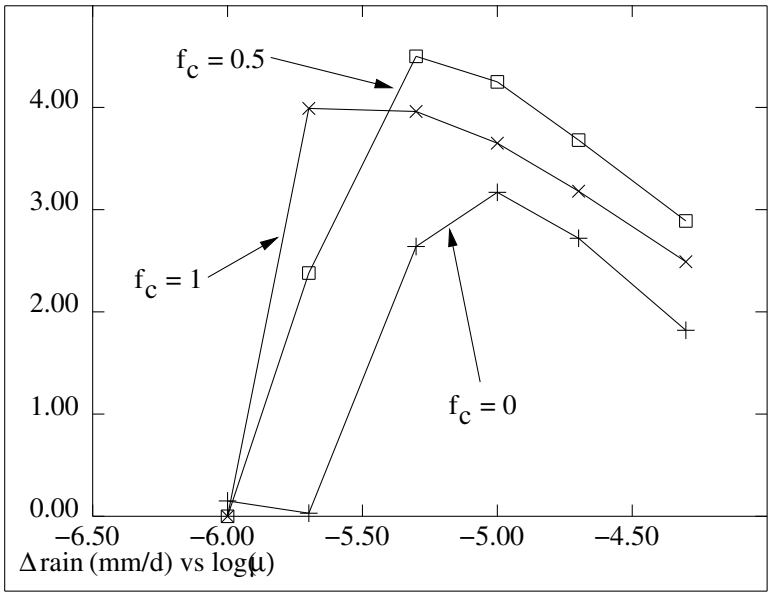


Figure 5: Difference between test column and reference column rainfall rates as a function of $\log(\mu)$ for all tested values of $f_c$.

sions are stable. For $\mu = 1 \times 10^{-6}$ ks km$^{-2}$, the parameter $\Delta x = 1/(\mu c) = 20000$ km if the gravity wave speed $c = 50$ m s$^{-1}$. Thus, circulations must have dimensions less than $10000 - 20000$ km for instability to exist in the model.

As $\mu$ increases, the difference between rainfall rates reaches a peak value and then begins to decline for all values of $f_c$. The reasons for this decrease are discussed below.

As noted earlier, the two-column calculation is only strictly valid if the difference between column buoyancies is small. Figure 6 shows the difference between the test and reference column potential temperatures, averaged over the height interval $3-12$ km, as a function of $\log(\mu)$. As $\mu$ increases, the difference between the two columns decreases for all values of $f_c$, indicating that the model results are most valid for the larger values of $\mu$, i. e., for smaller spatial scales.

Figure 7 shows the equilibrium horizontal wind between the two columns and the equilibrium vertical wind in the test column for the case $f_c = 0$ and $\mu = 20\times10^{-6}$ ks km$^{-2}$. The horizontal wind is obtained from the entrainment profile: $U = -\Delta x E/\rho$, where

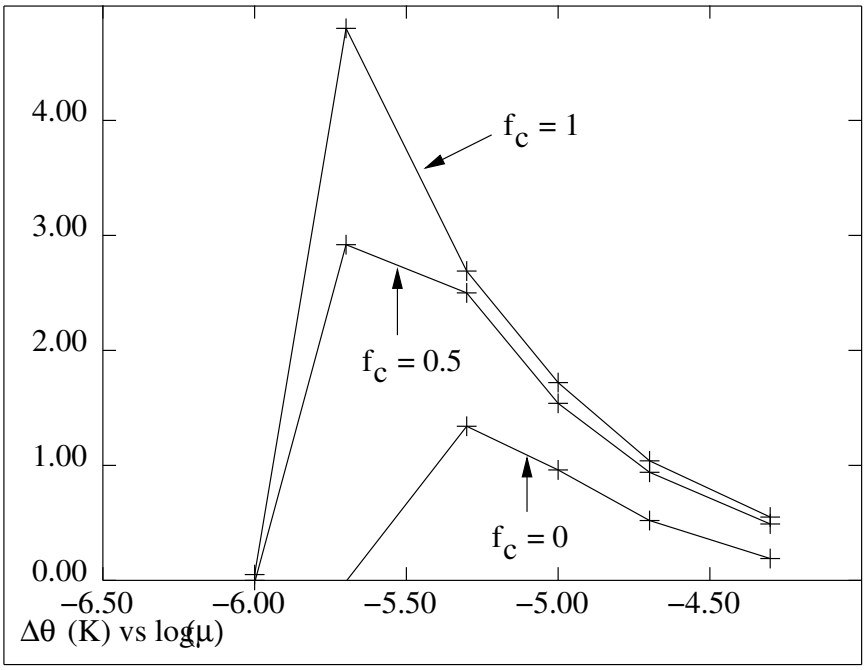


Figure 6: Difference between equilibrium potential temperatures in test and reference columns, averaged over $3 - 12$ km, as a function of $\log(\mu)$ for all values of $f_c$.

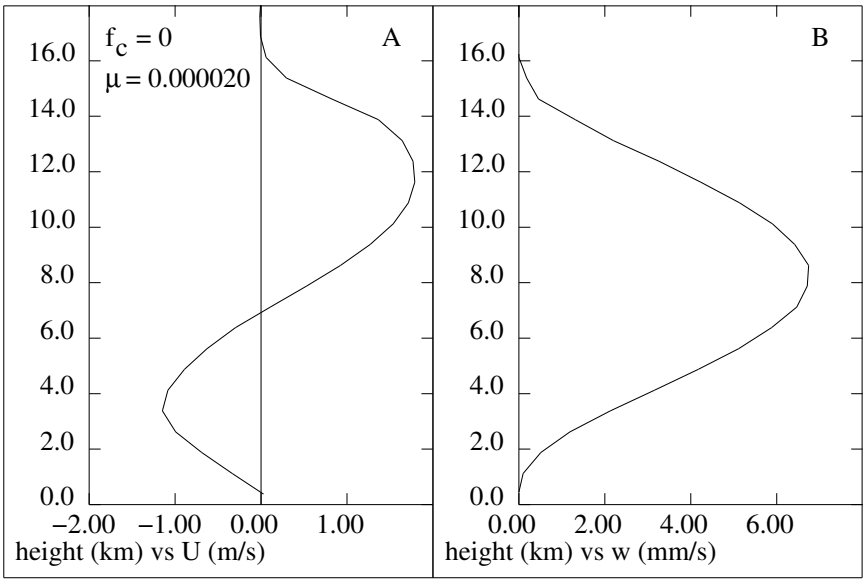


Figure 7: Equilibrium horizontal wind $U$ between the columns (left panel) and vertical wind in the test column (right panel) for $f_c = 0$ and $\mu = 20 \times 10^{-6}$ ks km$^{-2}$.

$\Delta x = 1/(\mu c) = 1000$ km. The level of non-divergence is of order $z = 7$ km and vertical velocities are comparable to radiative subsidence rates.

Figure 8 shows the vertical profiles of equilibrium equivalent potential temperature and saturated equivalent potential temperature in the test and reference columns for $f_c = 0$ and $\mu = 20 \times 10^{-6}$ ks km$^{-2}$. Note that the test column is slightly colder than the reference column up to about 4 km, as indicated by the profiles of saturated equivalent potential temperature. However, the test column is warmer than the reference column between 4 km and 12 km, and slightly colder from 12 km to the tropopause. More significantly, the test column is significantly moister than the reference column except at the surface, as indicated by the equivalent potential temperature profile. Since the rainfall rate in the test column exceeded that in the reference column, this result is in agreement with the hypothesis that more humid environments produce more rainfall.

All variables in the model are assigned cell-centered values. Surface values are obtained by linear extrapolation to the surface. Extrapolation of the cell-centered equiv-

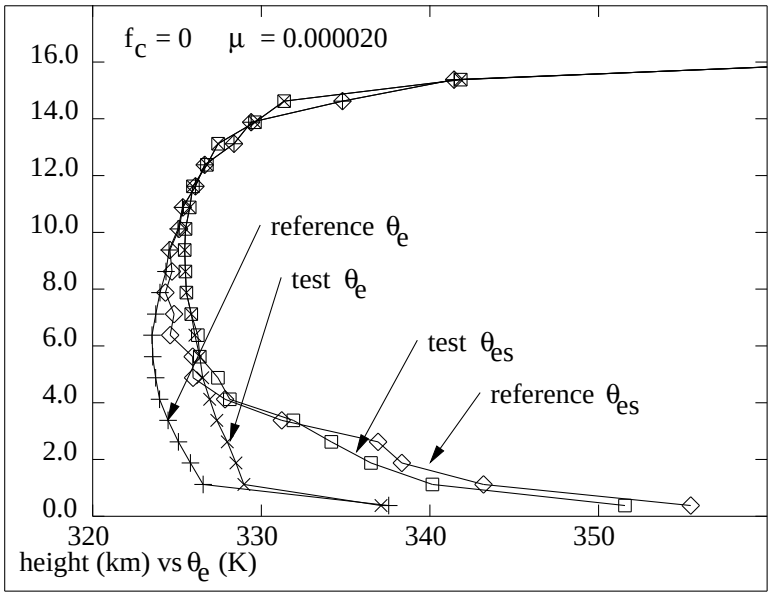


Figure 8: Equilibrium profiles of $\theta_e$ and $\theta_{es}$ in the test and reference columns for the case with $f_c = 0$ and $\mu = 20 \times 10^{-6}$ ks km$^{-2}$.

alent potential temperature values actually results in higher surface $\theta_e$ in the reference column than in the test column. This is physically interpreted to mean that weaker convective mixing in the reference column allows surface fluxes to build up higher values of surface or boundary layer equivalent potential temperatures.

The correlation between humidity and rainfall rate extends to all cases studied, as is seen in figure 9, which shows the equilibrium rainfall rate in both test and reference columns plotted versus the value of

$$\overline{\delta\theta_e} \equiv \frac{1}{b-a}\int_a^b (\theta_{es} - \theta_e)dz, \tag{23}$$

where $a = 1$ km and $b = 5$ km. The parameter $\overline{\delta\theta_e}$ is a measure of the saturation deficit in the altitude range over which significant precipitation formation takes place. The correlation between saturation deficit and rainfall rate is essentially built into the convective parameterization used in the present work, so this result doesn't come as a particular surprise. However, it does allow us to test the consequences of this hypothesis

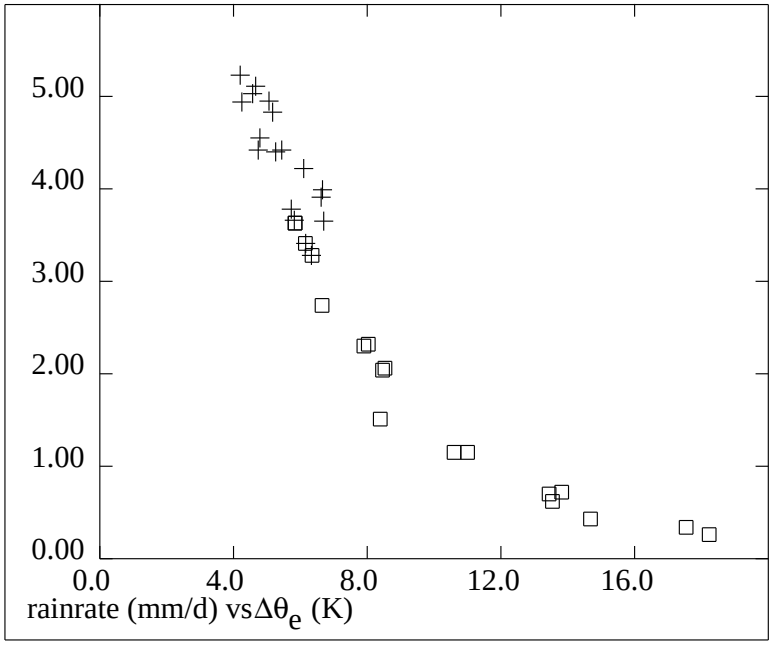


Figure 9: Equilibrium rainfall rate in test and reference columns plotted against $\overline{\delta\theta_e}$ for all test cases.

in the two-column model.

The above result allows us to clean up one loose end, namely, why the difference between test and reference column rainfall rates actually decreases when $\mu$ increases beyond a certain point. This apparently happens because the stronger coupling between the columns drives not only the temperature profiles, but also the humidity profiles in the two columns toward each other, which reduces $\overline{\delta\theta_e}$. However, since precipitation is so closely coupled to $\overline{\delta\theta_e}$ in the model, the rainfall differential between the columns decreases as well.

# 4 Analysis of instability

According to the analysis in the introduction, the budget of equivalent potential temperature should play a crucial role in the dynamics of the two-column system. In particular, the column with the larger net source of equivalent potential temperature due to surface fluxes and radiation should produce more rainfall than the other column, at least in a steady state. We now test the validity of this hypothesis in the model.

Vertical integration of equation (11) gives us the time tendency of the vertically integrated equivalent potential temperature in the test column:

$$\frac{d}{dt}\int_0^h \rho\theta_e dz = \int_0^h < \theta_e > E dz + \int_0^h \rho S_e dz \equiv \mathcal{E}_e + \mathcal{S}_e, \tag{24}$$

where we assume that $w = 0$ at the domain top, $z = h$. The first term on the right side of (24) represents the lateral import of entropy, $\mathcal{E}_e$, while the second, $\mathcal{S}_e$, is the net equivalent potential temperature source from radiation and surface fluxes.[1]

Figure 10 shows a time series of total (latent plus sensible) surface heat flux in the test and reference columns for the case $f_c = 0$ and $\mu = 20 \times 10^{-6}$ ks km$^{-2}$. The test column has stronger surface heat fluxes because the stronger deep convection in this column

[1]The model does not generate entropy in dissipative processes, so the equivalent potential temperature is not increased by dissipation. However, this possibility must be accounted for in the real world.

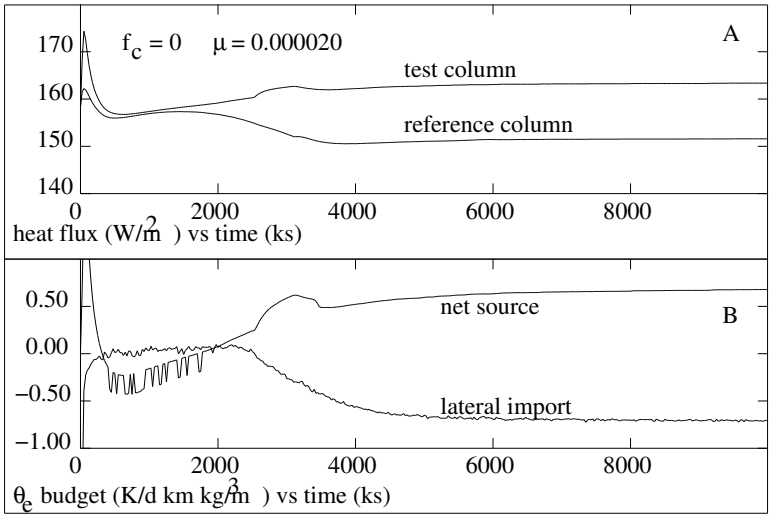


Figure 10: Time series of total surface heat flux in test and reference columns (upper panel) and the equivalent potential temperature import, $\mathcal{E}_e$, and generation, $\mathcal{S}_e$, in the test column (lower panel) for the case with $f_c = 0$ and $\mu = 20 \times 10^{-6}$ ks km$^{-2}$.

mixes down mid-level air with low equivalent potential temperature more effectively than in the reference column. This increases the difference between the boundary layer equivalent potential temperature $\theta_{eb}$, and the saturated sea surface equivalent potential temperature $\theta_{ess}$ in the bulk flux formula, thus enhancing the flux, $F_e$:

$$F_e = \rho C_D U_{eff}(\theta_{ess} - \theta_{eb}). \tag{25}$$

The effective surface wind $U_{eff}$ is held fixed at 5 m s$^{-1}$ in both columns (see table 1).

The generation of entropy by surface fluxes dominates radiative effects in this case, as the radiative differences between the two columns, which are driven solely by differences in water vapor profiles, are small. Thus, the enhanced surface fluxes cause the net entropy source $\mathcal{S}_e$ to be positive, as figure 10 shows. The lateral import of entropy $\mathcal{E}_e$ comes into balance with this source, and thus takes on negative values, which means that entropy is being exported from the test to the reference column, as envisioned by Neelin and Held (1987). It is interesting that an excess surface heat flux of only about 10 W m$^{-2}$ is needed to drive the two-column circulation in this case.

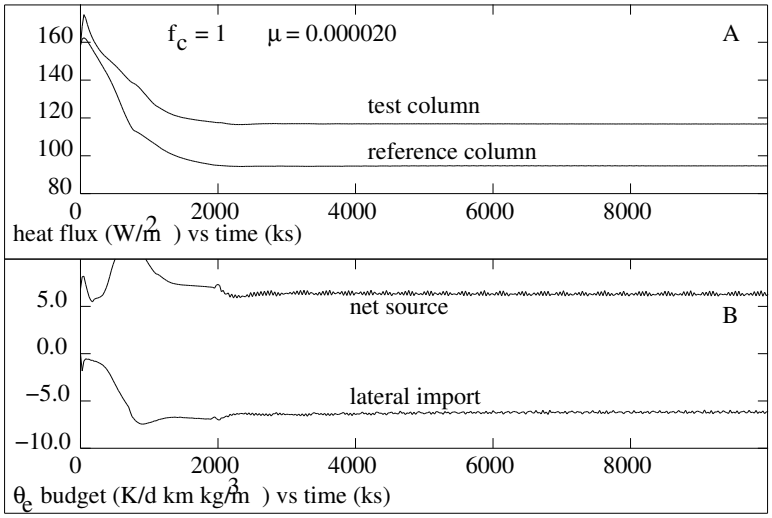


Figure 11: As in figure 10 except for $f_c = 1$.

Figure 11 shows the corresponding plots for the case with $f_c = 1$ and $\mu = 20 \times 10^{-6}$ ks km$^{-2}$, i. e., with 100% cloud fraction. The test column minus reference column surface heat flux in this case is about 20 W m$^{-2}$, or about twice that in the corresponding case with $f_c = 0$. Thus, the cloud radiation effects are acting indirectly to double the differential surface heat flux between the columns. However, the biggest difference between the $f_c = 0$ and $f_c = 1$ cases is the vast increase in the net production of entropy in the test column. This grossly exceeds that explainable by the relative increase in surface heat flux, and must be attributed to cloud-radiation interactions in the model.

This conclusion is confirmed by figure 12, which shows the radiative and convective sources of equivalent potential temperature in the test column for the two cases discussed above. Absorption near the mid-level bases of stratiform cloudiness is clearly evident, as is the (probably too strong) absorption of solar radiation at high levels.

The gross moist stability (GMS) for these circulations may be calculated as follows:

$$\text{GMS} = -\int_0^d < \theta_e > E dz \Big/ \int_{E>0} E dz \; . \tag{26}$$

Figure 13 shows the variation of the GMS with $\mu$ for the three different values of $f_c$. The GMS increases by almost an order of magnitude as the fractional cloud cover increases

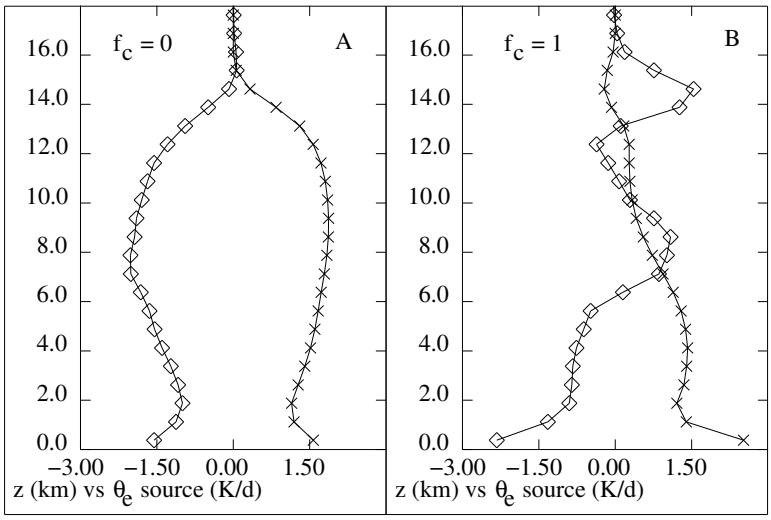


Figure 12: Equilibrium radiative (diamonds) and convective (crosses) sources of equivalent potential temperature as a function of height for $\mu = 20 \times 10^{-6}$ ks km$^{-2}$ and for $f_c = 0$ (left panel) and $f_c = 1$ (right panel).

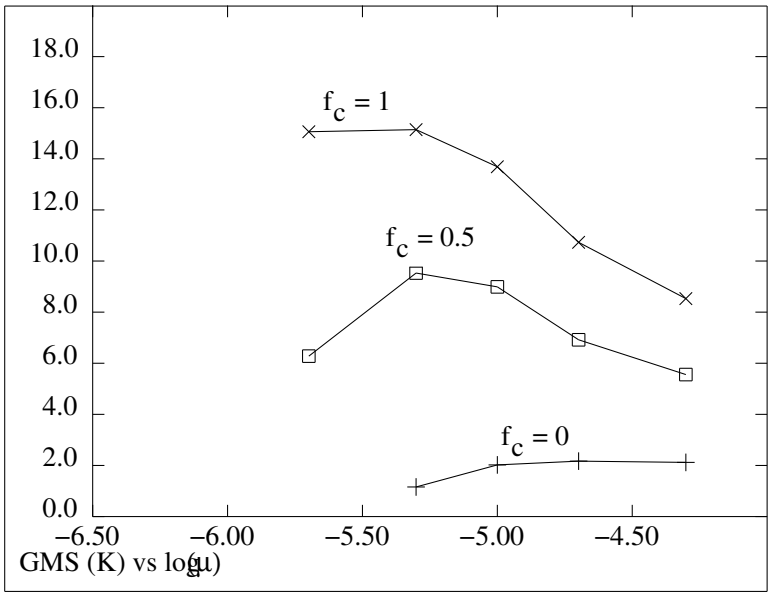


Figure 13: Gross moist stability (GMS) as a function of $\log(\mu)$ for $f_c = (0, 0.5, 1.0)$.

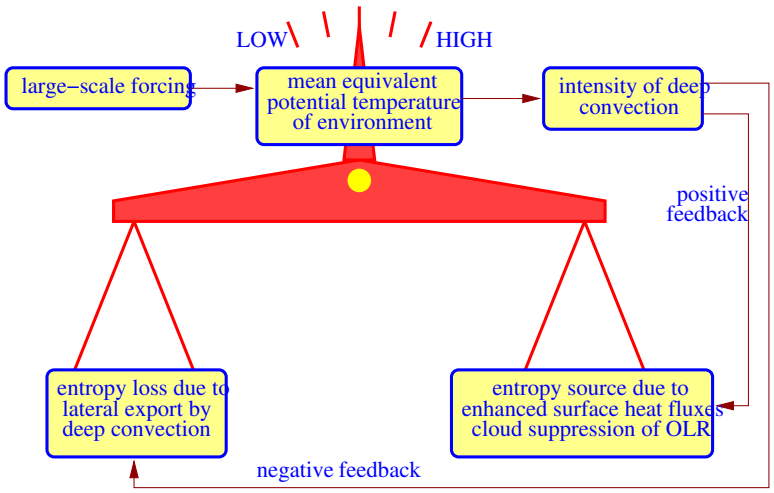


Figure 14: Hypothesized factors affecting the balance of equivalent potential temperature in the tropical atmosphere.

from zero to unity. This reflects the role of middle to upper level stratiform clouds in reducing the outgoing longwave radiative flux.

# 5 Conclusions and discussion

Figure 14 summarizes our conclusions about the factors which control the mean equivalent potential temperature of the tropical troposphere, and indirectly the intensity of deep convection and rainfall there. The mean equivalent potential temperature in a column is the result of a balance between the $\theta_e$ tendency due to surface fluxes and cloud-radiation interactions on the one hand, and the lateral export of high equivalent potential temperature air by convection on the other hand.

The negative feedback in figure 14 results from the assumed sensitivity of rainfall production to environmental equivalent potential temperature — if the mean environmental $\theta_e$ becomes too large, rainfall increases and convective circulations become more intense, resulting in enhanced lateral export and reduction in the environmental $\theta_e$. Negative excursions of mean $\theta_e$ have the opposite effect. If negative feedback dominates, then the

amount of convection and rainfall becomes a smooth function of external forcing, i. e., the large scale anomaly in the net source of equivalent potential temperature.

The positive feedback comes from the tendency of deep convection to enhance local surface heat fluxes by virtue of downdraft production, and to locally suppress outgoing longwave radiation as a result of the creation of stratiform cloudiness. Whether instability or stability occurs in the column depends on the relative weights of the positive and negative feedbacks. For the present model, positive effects outweigh negative, resulting in instability, which means that convection and rainfall in a column are not a unique function of external forcing.

The above conclusions apply only to the two-column model with the particular choice of diabatic parameterizations used. In order to make inferences about the real world, the limitations of the model must be understood.

The two-column model reduces large scale tropical dynamics to its simplest elements, eliminating in particular any effects of the Coriolis force and quasi-balanced dynamics. The calculations reported here are also limited to equal SSTs in the two columns. The results are thus applicable primarily to regions of nearly uniform SST very near the equator, such as the west Pacific warm pool. A further limitation is the inability of the model to produce differing ambient winds in the two columns in response to the dynamics of the flow. This has a large effect on the ability of the model to reproduce actual surface heat fluxes.

The convective parameterization exhibits a very strong relationship between environmental humidity and precipitation rate, as illustrated in figure 9. The possible effects of wind shear, aerosol concentration, etc., on precipitation are not accounted for. This relationship needs to be tested extensively both by modeling and by observation before it can be accepted with confidence.

The radiation parameterization also has significant deficiencies, particularly in the treatment of shortwave radiation. In addition, the treatment of sub-grid-scale variability in cloudiness is crude. In spite of these limitations, the qualitative effect of clouds

on radiation would seem to be adequately represented by the model, with the biggest uncertainties arising from predictions of the distribution of stratiform clouds by the convective parameterization and the net radiative energy balance in the upper parts of stratiform clouds.

In spite of the above limitations, the idea that convection and precipitation over warm tropical oceans are driven by anomalies in the source of equivalent potential temperature would appear to be a model-independent hypothesis worth testing in further computational and observational work. In particular, the notion that convection can induce an instability by virtue of its own effects on surface heat fluxes and outgoing longwave radiation is particularly appealing as a way to explain the observed patchy nature of deep convection over the warm equatorial oceans.

*Acknowledgments.* This work was supported by National Science Foundation Grant ATM-9616290 and NOAA Office of Global Programs Grant NA56GP0219.

# 6 References

Albrecht, B., and S. K. Cox, 1975: The large-scale response of the tropical atmosphere to cloud modulated infrared heating. *J. Atmos. Sci.,* **32,** 16-24.

Arakawa, A., and W. H. Schubert, 1974: Interaction of a cumulus cloud ensemble with the large-scale environment, Part I. *J. Atmos. Sci.,* **31,** 674-701.

Cess, R. D., M. H. Zhang, P. Minnis, L. Corsetti, E. G. Dutton, B. W. Forgan, D. P. Garber, W. L. Gates, J. J. Hack, E. F. Harrison, X. Jing, J. T. Kiehl, C. N. Long, J.-J. Morcrette, G. L. Potter, V. Ramanathan, B. Subasilar, C. H. Whitlock, D. F. Young, and Y. Zhou, 1995: Absorption of solar radiation by clouds: Observations versus models. *Science,* **267,** 496-499.

Cess, R. D., M. H. Zhang, F. P. J. Valero, S. K. Pope, A. Bucholtz, B. Bush, C. S. Zender, and J. Vitko, 1999: Absorption of solar radiation by the cloudy atmo-

sphere: Further interpretations of collocated aircraft measurements. *J. Geophys. Res.,* **104,** 2059-2066.

Cess, R. D., and M. H. Zhang, 1996: How much solar radiation do clouds absorb: Response. *Science,* **271,** 1133-1134.

Chao, W. C., and S.-J. Lin, 1994: Tropical intraseasonal oscillation, super cloud clusters, and cumulus convection schemes. *J. Atmos. Sci.,* **51,** 1282-1297.

Cox, S. K., and K. T. Griffith, 1979: Estimates of radiative divergence during Phase III of the GARP Atlantic Tropical Experiment: Part II. Analysis of Phase III results. *J. Atmos. Sci.,* **36,** 586-601.

Ferrier, B. S., J. Simpson, and W.-K. Tao, 1996: Factors responsible for precipitation efficiencies in midlatitude and tropical squall simulations. *Mon. Wea. Rev.,* **124,** 2100-2125.

Gray, W. M., 1973: Cumulus, convection and larger scale circulations. Part I: Broad-scale and mesoscale considerations. *Mon. Wea. Rev.,* **101,** 839-855.

Liou, K.-N., 1980: *An introduction to atmospheric radiation.* Academic Press, 392 pp.

Mapes, B. E., 1993: Gregarious tropical convection. *J. Atmos. Sci.,* **50,** 2026-2037.

Neelin, J. D., and I. M. Held, 1987: Modeling tropical convergence based on the moist static energy budget. *Mon. Wea. Rev.,* **115,** 3-12.

Nilsson, J., and K. A. Emanuel, 1999: Equilibrium atmospheres of a two-column radiative-convective model. *Quart. J. Roy. Meteor. Soc.,* **125,** 2239-2264.

Pierrehumbert, R. T., 1995: Thermostats, radiator fins, and the local runaway greenhouse. *J. Atmos. Sci.,* **52,** 1784-1806.

Ramanathan, V., B. Subasilar, G. J. Zhang, W. Conant, R. D. Cess, J. T. Kiehl, H. Grassl, and L. Shi, 1995: Warm pool heat budget and shortwave cloud forcing: A missing physics? *Science,* **267,** 499-503.

Raymond, D. J., 1994: Convective processes and tropical atmospheric circulations. *Quart. J. Roy. Meteor. Soc.,* **120,** 1431-1455.

Raymond, D. J., 1995: Regulation of moist convection over the west Pacific warm pool. *J. Atmos. Sci.,* **52,** 3945-3959.

Raymond, D. J., 2000a: The Hadley circulation as a radiative-convective instability. *J. Atmos. Sci*, (in press).

Raymond, D. J., 2000b: The thermodynamic control of tropical rainfall. *Quart. J. Roy. Meteor. Soc.*, (in press).

Raymond, D. J., and D. J. Torres, 1998: Fundamental moist modes of the equatorial troposphere. *J. Atmos. Sci.,* **55,** 1771-1790.

Rotunno, R., and J. Klemp, 1985: On the rotation and propagation of simulated supercell thunderstorms. *J. Atmos. Sci.,* **42,** 271-292.

Rotunno, R., J. B. Klemp, and M. L. Weisman, 1988: A theory for strong, long-lived squall lines. *J. Atmos. Sci.,* **45,** 463-485.

Smolarkiewicz, P. K., 1983: A simple positive definite advection scheme with small implicit diffusion. *Mon. Wea. Rev.,* **111,** 479-486.

Stephens, G. L., 1996: How much solar radiation do clouds absorb. *Science,* **271,** 1131-1133.

Valero, F. P. J., R. D. Cess, M. H. Zhang, S. K. Pope, A. Bucholtz, B. Bush, and J. Vitko, 1997: Absorption of solar radiation by the cloudy atmosphere: Interpretations of collocated aircraft measurements. *J. Geophys. Res.,* **102,** 29917-29927.

Waliser, D. E., and N. E. Graham, 1993: Convective cloud systems and warm-pool surface temperatures: Coupled interactions and self-regulation. *J. Geophys. Res.,* **98,** 12881-12893.

Xu, K.-M., and A. Arakawa, 1992: Semiprognostic tests of the Arakawa-Schubert cumulus parameterization using simulated data. *J. Atmos. Sci.,* **49,** 2421-2436.

Xu, K.-M., A. Arakawa, and S. K. Krueger, 1992: The macroscopic behavior of cumulus ensembles simulated by a cumulus ensemble model. *J. Atmos. Sci.,* **49,** 2402-2420.

Yano, J.-I., J. C. McWilliams, and M. W. Moncrieff, 1996: Fractality in idealized simulations of large-scale tropical cloud systems. *Mon. Wea. Rev.,* **124,** 838-848.

Yano, J.-I., J. C. McWilliams, M. W. Moncrieff, and K. A. Emanuel, 1995: Hierarchical tropical cloud systems in an analog shallow-water model. *J. Atmos. Sci.,* **52,** 1723-1742.

Zipser, E. J., 1969: The role of organized unsaturated convective downdrafts in the structure and rapid decay of an equatorial disturbance. *J. Appl. Meteor.,* **8,** 799-814.